Presentation

POST-FLIGHT AEROTHERMAL ANALYSIS OF HUYGENS PROBE

Michael J. Wright[(1)], Brian R. Hollis[(2)], Deepak Bose[(3)], Louis Walpot[(4)]

[(1)] NASA Ames, MS 230-2, Moffett Field, CA 94035, Michael.J.Wright@nasa.gov
[(2)] NASA Langley, MS XX-X, Hampton, VA 23681, Brian.R.Hollis@nasa.gov
[(3)] ELORET Corp., MS 230-3, Moffett Field, CA 94035, dbose@mail.arc.nasa.gov
[(4)] AOES B.V., Netherlands, Louis.Walpot@aoes.com

ABSTRACT

The design aeroheating environment for the Huygens probe is briefly reviewed. New aeroheating calculations are then performed for the Huygens Probe during its entry to Titan, based on new convective and radiative heating models developed in the last two years by the NASA In-Space Propulsion program to explore possible Titan aerocapture missions. The calculations are carried out on a Monte-Carlo predicted worst-case peak heating trajectory assuming a standard minimum density atmospheric profile. Despite the differences in physical and atmosphere modeling, the convective heating results from these new calculations are in good agreement with the design values. On the other hand, the new predictions of radiative heating are significantly lower than those computed during probe design.

1. INTRODUCTION

The highly successful entry and landing of the European Space Agency's (ESA) Huygens probe on the surface of Titan on January 14, 2005 has generated renewed interest in further exploration of this Saturnian moon. From an entry, descent and landing (EDL) standpoint one of the primary technical challenges to future Titan entries is the aerothermal environment encountered by the entering probe and the resulting thermal protection system (TPS) selection and sizing.

Although the entry velocity of the Huygens probe was not large (V_∞ = 6.2 km/s), pre-flight analysis predicted high heating rates to the vehicle, with 50% or more of the total due to shock layer radiation. This radiation is a direct result of the unique chemical composition of Titan's atmosphere, which is composed primarily of nitrogen with a small amount of methane. When this gas mixture is shocked a large amount of CN is produced, which is a strong radiator in the violet and red portions of the spectrum. In general, this shock layer radiation is produced via a nonequilibrium process governed by rates that must be determined from experimental data. However, due to a lack of suitable validation data for CN radiation, prior analyses of the Huygens entry assumed either an equilibrium (Boltzmann) [1] or an unvalidated nonequilibrium model [2-3]. These assumptions led to large uncertainties in the radiative heating environment.

Recently, a series of shock tube tests were conducted at shock velocities between 5-10 km/s in a Titan gas mixture to obtain validation data for shock layer radiation codes [4]. These tests provided the first set of fully calibrated spectrally resolved CN violet radiation data in the critical 13-133 Pa pressure regime that is most representative of the Huygens entry environment. These data indicate that the equilibrium (Boltzmann) model overpredicts the radiative heating by a factor of 2-7. A new collisional-radiative model was developed based on these data [4]; this model will be used to estimate the radiative heating environment seen by the probe.

A primary contributor to the predicted convective heating rate is wall catalysis, particularly the recombination of hydrogen atoms on the surface. Although CH_4 is a trace species in the Titan atmosphere, it is quickly decomposed behind the shock. Each CH_4 molecule releases four hydrogen atoms into the shock layer, which quickly diffuse to the surface due to their high mobility. Accurate modeling of this diffusion process is required to accurately predict the flux of hydrogen atoms reaching the surface and the resulting energy released by catalytic recombination to form H_2. Another important consideration is transition to turbulence. Unlike previous planetary probes, the Huygens heat shield is tiled. Tile gaps will lead to a distributed roughness pattern on the surface even prior to the onset of ablation. This roughness may induce turbulent transition early in the trajectory, which must be accounted for.

The current paper first reviews the design aeroheating environments and then presents new computations based on the latest available high fidelity models for convective and radiative aeroheating. Results are presented only for the forebody at zero degrees angle of attack (ballistic entry).

Proc. '3rd International Workshop Planetary Probe', Anavyssos, Attiki, Greece, 27 June – 1 July 2005 (ESA SP-607, April 2006)

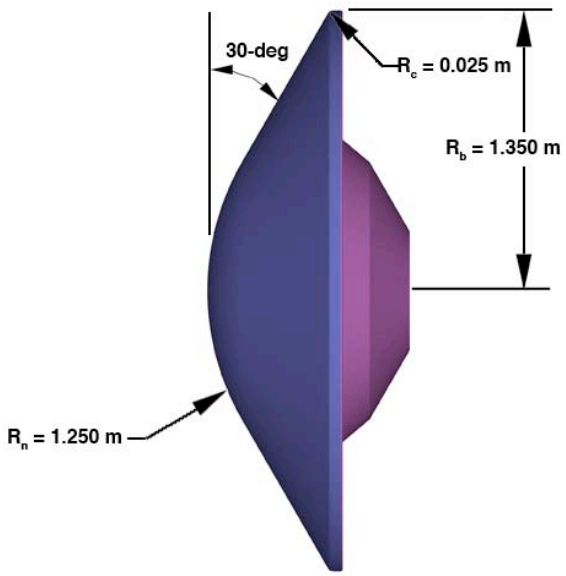

Fig. 1. Schematic diagram of Huygens entry probe.

2. HUYGENS PROBE GEOMETRY

The Huygens probe, shown schematically in Fig. 1, was a 60° half-angle sphere-cone with a diameter of 2.7 m and a nose radius of 1.25 m. The forebody heatshield thermal protection system (TPS) was composed of AQ60, an ablative material that is blend of silica fibers reinforced by phenolic resin. AQ60 was applied in tiles to the forebody of the vehicle. The open backshell design of the probe (see Fig. 1) had the consequence that approximately half of the conical frustum was exposed to potentially hot boundary layer gases from both sides during entry.

3. REVIEW OF DESIGN AEROHEATING

Design aeroheating environments for the Huygens probe were reported in the open literature by Baillion et al. [2-3, 5] The Huygens probe was assumed to enter the atmosphere of Titan on a ballistic trajectory at a relative velocity of 6.19 km/s and a nominal flight path angle of γ = -64°. The atmospheric composition was assumed to consist primarily of nitrogen, with up to 5% methane and 20% argon by volume. The worst-case combined heating was predicted to occur in an atmosphere that consisted of 3.5% methane and 20% argon [2]. Flight path angle variations between -60° and -66° were considered. Two key TPS sizing locations were identified on the forebody: the stagnation point and the mid-cone point (halfway between the sphere-cone junction and shoulder). The mid-cone location was chosen both to capture the effects of possible transition to turbulence, and also because this location lies on the exposed portion of the frustum (see Fig. 1), at which heating on both sides of the frustum impacted the substructure thermal analysis.

Convective heating was computed using a finite-rate thermo-chemical nonequilibrium CFD solver. The Nelson kinetic model [6] was used for the chemical reaction rates. The surface of the probe was assumed to be fully catalytic and in radiative equilibrium. Ordinary diffusion was modeled assuming a constant Lewis number (Le = 1.4) for all species. Turbulent transition was predicted to occur late in the trajectory (after peak heating), but the computed turbulent heat fluxes on the frustum were not predicted to exceed the laminar stagnation point value. The predicted peak stagnation point convective heat fluxes ranged from 40–50 W/cm^2, and had an assumed uncertainty of ±10% [5].

Radiative heating was computed using a quasi-steady state (QSS) nonequilibrium model. This model, discussed in [2], assumes that excitation of the CN molecule is governed by electron collisions. The effects of excitation via absorption, as well as the non-adiabatic effects of energy converted to radiation (radiative cooling), were neglected. This model was shown to provide reasonable agreement with the shock tube data of Park [7]. However, the data of Park were obtained at an ambient pressure of 266 Pa, which is more than an order of magnitude higher than the pressure at the peak radiative heating point in flight (15 Pa at 5.1 km/s). In addition, the Nelson kinetic model has since been shown to significantly overpredict ionization levels (and therefore electron number density) in the flow [8]. A correction factor of 0.8 was applied to the 1D line of sight radiative heating results to account for shock layer curvature effects. The predicted peak stagnation point radiative heat flux using this model ranged from 35–50 W/cm^2, and had an assumed uncertainty of ±75% [5] It should be noted that the radiation model predicted that radiative heating would be strongly sensitive to the level of atmospheric Argon [2]. However, this result was later contradicted by shock tube test data [9].

Design heat loads (combined radiative and convective), including uncertainties, were between 3500-4000 J/cm^2 at the stagnation point.

4. ENTRY TRAJECTORY AND ATMOSPHERE

It was hoped that the current analysis could be applied to the actual reconstructed entry trajectory of the Huygens probe. However, such trajectory information is not yet available. Therefore, the analysis herein is carried out using a Monte-Carlo trajectory developed at

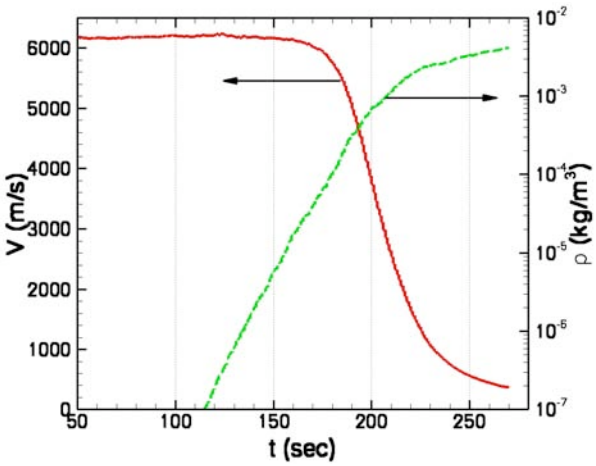

Fig. 2. Nov. 11 NESC peak heating trajectory.

NASA Langley during the National Engineering Safety Center (NESC) independent assessment of the Huygens EDL system conducted prior to the probe release in 2004. Details of the trajectory and analysis performed during this investigation are given in [1].

Time histories of atmospheric density and velocity along the trajectory employed, known as the Nov. 11 peak heat rate trajectory, are shown in Fig. 2. Atmospheric temperature and density as a function of altitude are taken from the TitanGRAM model [10]. This model was developed during NASA's 2003 Titan aerocapture system study [11] and updated in 2004 to incorporate profile and composition data obtained during the Cassini T0 and TA passes.

The radiative heating encountered during entry is predicted to be a strong function of the amount of CH_4 in the atmosphere. Early estimates of this value ranged up to 9% by volume. In addition, Argon was thought to be present in concentrations up to 20% by volume. However, the recent Cassini flybys have thus far indicated an atmosphere consisting of about 1.8 ± 0.5% CH_4 by volume at entry altitudes. Argon has not been definitively detected, but its presence at low levels is inferred. Since at low concentrations the amount of shock layer radiation produced is directly proportional to the amount of methane in the freestream, the analysis herein is conducted assuming the maximum (worst case) methane concentration, which results in a mixture of 97%, N_2, 2.3% CH_4, and 0.7% Ar by volume.

5. SIMULATION METHODOLOGY

Computational Fluid Dynamics (CFD) simulations are performed using three separate tools: DPLR [12] at NASA Ames, LAURA [13] at NASA Langley, and LORE [14] at AOES. In each case a consistent set of physical models is employed, as discussed in this section. Steady-state solutions are obtained with each code at a number of points along the Nov. 11 trajectory assuming a worst-case methane composition as discussed above. Table 1 lists the relevant conditions for the nine trajectory points considered.

Table 1. Trajectory points simulated.

t (sec)	ρ_∞ (kg/m^3)	V_∞ (m/s)	T_∞ (K)
151	6.22×10^{-6}	6167	179.0
169	3.64×10^{-5}	6049	171.3
177	7.20×10^{-5}	5886	175.8
185	1.83×10^{-4}	5490	177.0
189	2.96×10^{-4}	5126	176.6
193	3.79×10^{-4}	4705	175.8
201	7.43×10^{-4}	3660	173.4
209	1.11×10^{-3}	2694	170.9
225	2.25×10^{-3}	1338	167.1

Each CFD code solves the reacting Navier-Stokes equations assuming the gas is in thermochemical non-equilibrium. In addition to mass (for each species) and momentum conservation equations, two energy equations are solved; a total energy equation and a vibro-electronic energy equation. In this formulation it is assumed that the vibrational and electronic modes of the gas are in equilibrium with each other, but not with the translational-rotational component. This model was originally developed for air flows, but should be a reasonable approximation for the N_2-dominated Titan atmosphere as well. Details of the equations employed and the required source term and energy exchange models are given in [15-16].

At the entry velocities considered, the amount of ionization is small enough (< 0.1%) that its effect on convective heating is negligible. In addition, the results of Bose et al. [4] have demonstrated that electron impact excitation collisions are not a major contributor to nonequilibrium radiation. Therefore a 14-species (CH_4, CH_3, CH_2, HCN, N_2, C_2, H_2, CH, NH, CN, N, C, H, Ar) 26-reaction finite-rate chemistry model is used in this paper. However, for completeness one case is run using a 21-species 34-reaction model, including the ions N_2^+, CN^+, N^+, C^+, H^+, and Ar^+ as well as free electrons. In each case the reaction rates are taken from Gökçen [8]. This model was developed to incorporate recently published kinetic rate data for several reactions that was not available to Nelson et al. [6], and was shown to accurately reproduce available shock tube data [8].

Viscosity and thermal conductivity are modeled using the species expressions and mixing rules presented by Gupta et al. [17] The self-consistent effective binary diffusion (SCEBD) method [18] or its equivalent [19] is used to model mass diffusion fluxes. The surface is assumed to be fully catalytic to all ions, N_2 and H_2 recombination (DPLR & LORE), or supercatalytic (LAURA). A radiative equilibrium boundary condition is applied, with a constant emissivity of 0.85.

Either a laminar or fully turbulent flow model is used, depending on the case. For turbulent flows, the compressible Baldwin-Lomax algebraic model [20] is implemented with a turbulent Schmidt number of 0.7 and a turbulent Prandtl number of 0.9. The flow field is assumed to transition to turbulence when the momentum thickness Reynolds number divided by the edge Mach number (Re_θ/M_e) exceeds 150, [1] a conservative value based on ground test data for the Mars Science Laboratory [21] chosen to account for possible early transition due to distributed roughness from ablation and steps and gaps between the TPS tiles.

Radiative heat fluxes are computed along one-dimensional lines of sight with two codes: NEQAIR96 [22] at NASA Ames and RADEQUIL [23] at NASA Langley. NEQAIR96 computes emission and absorption of atoms and molecules on a line-by-line (spectrally resolved) basis, while RADEQUIL uses a computationally efficient smeared-band model for molecular systems. Each code solves the radiative transport in one-dimension, with analytical corrections for a curved stagnation point geometry. Preliminary computations are made assuming that the CN molecule is the primary radiator (although radiation from other species is also considered) and that the distribution of excited states is Boltzmann, governed by the mixture vibrational-electronic temperature. This methodology is described in [24]. These computations, which also include the effect of absorption, should place an upper bound on the possible heat flux due to radiation.

In addition, computations are made at each point using the new non-local collisional-radiative (CR) model under development by Bose et al. [4], which was validated with shock tube tests conducted at the Electric Arc Shock Tube (EAST) facility at NASA Ames. This model, which includes collisional excitation and de-excitation of CN from the ground state to the B and higher states, ionization from the B-state, spontaneous emission, and absorption, was shown [4] to agree well with experimental data at 133 Pa. At lower pressure (~13 Pa) the CR model predicted the peak non-equilibrium emission rate correctly, but underpredicted the rate of decay to the equilibrium value. However, the CR model was in much better agreement with the experimental data than the equilibrium model.

It is not sufficient to simply compute the radiation in an uncoupled simulation, because this ignores the effects of radiative cooling (flowfield-radiation coupling). For the cases considered in this work, absorption effects are significant. Therefore, the methodology proposed by Wright et al. [25] to account for coupling cannot be employed directly. However, the impact of coupling on radiative heating can be estimated using the Tauber-Wakefield expression [26], given by

$$q^R_{coup} = q^R_{unc} / \left(1 + \kappa \Gamma^{0.7}\right) \tag{1}$$

where q^R_{coup} is the coupled radiative heat flux, q^R_{unc} is the corresponding uncoupled value, κ is a mixture specific constant equal to about 2 for Titan [25], and Γ is the Goulard number [27], given by

$$\Gamma = 2q^R_{unc} / (\tfrac{1}{2}\rho_\infty V_\infty^3) \tag{2}$$

where ρ_∞ and V_∞ are the freestream density and velocity, respectively. The potential increase in convective heating due to boundary layer absorption of shock layer radiation (and the resulting temperature increase) is not included in this analysis.

Finally, 1D stagnation point results are multiplied by a constant factor of 0.75 at the stagnation point and 1.0 on the flank to account for shock layer curvature effects. These values are consistent with that used for the Huygens design, [2] and were found to be appropriate for Huygens based on a limited amount of multi-dimensional analysis using a view factor approach [28].

6. RESULTS

Computed translational temperature and Mach number in the symmetry plane at the peak heating point (t = 189 s) are shown in Fig. 3. The peak temperature of about 10000 K occurs just behind the shock at the nose, but shock layer temperatures over most of the body are in the range of 5000-8000 K. The Mach number plot shows that the flow remains slightly subsonic at the boundary layer edge over the entire forebody, indicating that a 60° cone angle is very close to the critical value (at which the sonic point jumps from the sphere-cone junction to the shoulder) at this condition. It should be noted that movement of the sonic attachment point during entry was shown to cause slight aerodynamic instabilities during the Mars Pathfinder entry [29]. At

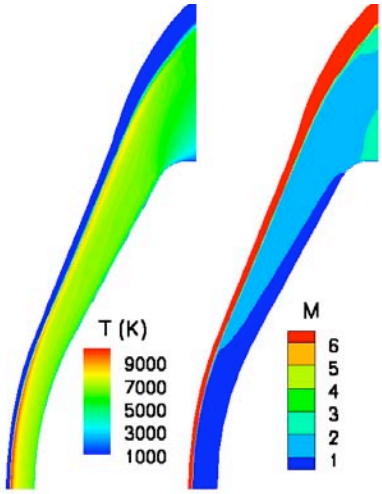

Fig. 3. Computed (a) translational temperature and (b) Mach number at t = 189 s.

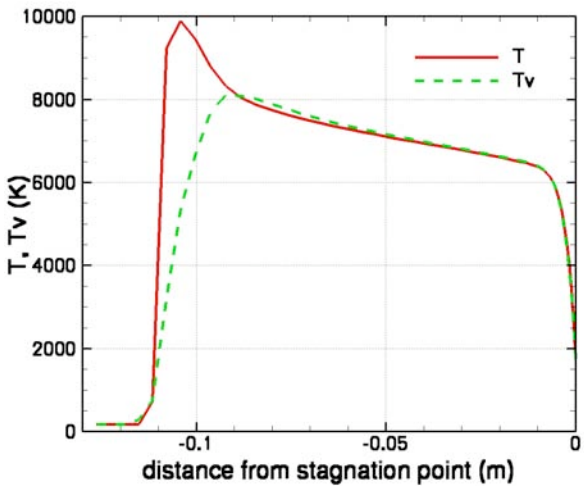

Fig. 4. Computed temperatures along the stagnation streamline at t = 189 s.

this time it is not known if similar instabilities were observed during the Huygens entry.

Fig. 4 shows the computed translational and vibro-electronic temperature along the stagnation streamline at the peak heating point. The predicted shock standoff distance at this time is about 11 cm. The translational temperature reaches a maximum of 10000 K, while the vibro-electronic peak temperature is about 8000 K. From the figure we see that most of the flowfield is in thermal equilibrium ($T \approx T_v$), with the exception of a 2 cm layer behind the shock. However, the entire shock layer is in chemical non-equilibrium, as can be seen by the gradual decrease in temperature from the shock to the boundary layer edge due to chemical reactions.

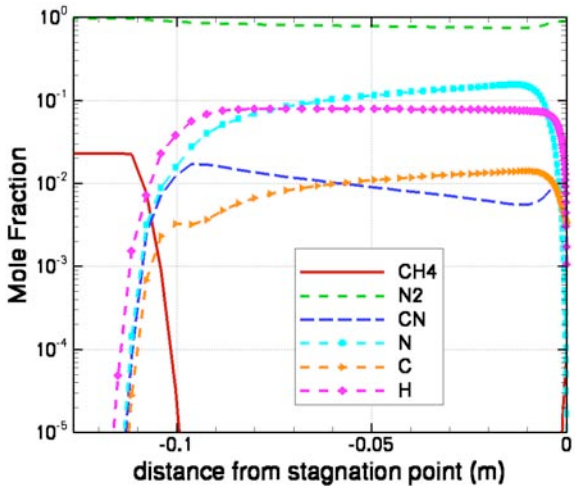

Fig. 5. Computed mole fractions along the stagnation streamline at t = 189 s.

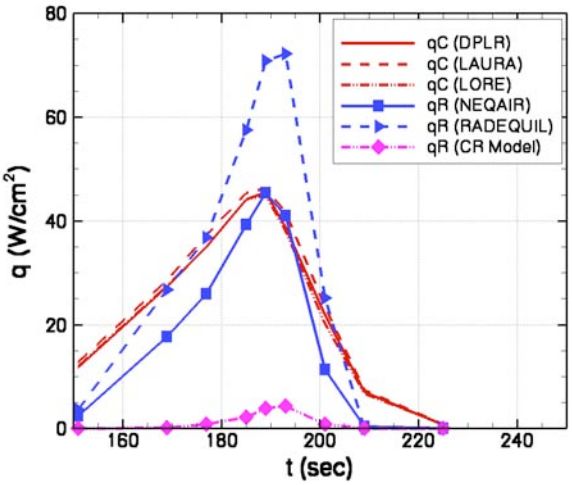

Fig. 6. Computed convective and radiative heating at the stagnation point along the Nov. 11 trajectory.

Fig. 5 shows the computed mole fractions of several key species along the stagnation streamline at the peak heating point. From the figure we see that the freestream methane is almost instantly dissociated by the shock layer. The N_2, on the other hand, is only about 10% dissociated at these conditions, and remains the dominant post-shock species. N and H atoms each exist in mole fractions about 0.1 behind the shock wave. The most important post-shock species from a radiation standpoint is the CN molecule, which reaches a peak mole fraction of about 0.02 behind the shock wave and then decreases slowly from the shock to the boundary layer edge. The peak mole fraction of CN roughly coincides with the location of peak vibro-electronic temperature, which implies that the strongest CN emission should occur in this region. It is important to

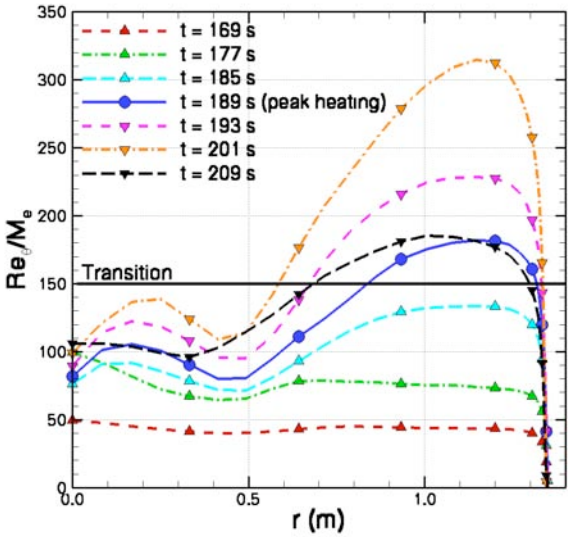

Fig. 7. Computed Re_θ/M_e as a function of distance from the stagnation point.

note that the mole fraction of CN actually increases somewhat near the body surface. In addition, the density of the gas also increases in this region, leading to high CN number densities in the boundary layer. This high concentration of cool CN molecules is a significant absorber of radiation from the shock layer.

6.1 Stagnation Point Heating

Fig. 6 shows the computed convective heating at the stagnation point on all nine trajectory points for the DPLR, LAURA, and LORE solutions. All three codes predict similar convective heating profiles, with a maximum difference of about 10%. This result is not surprising since all three codes use very similar physical models and assumptions (as agreed upon by a combined NASA/ESA aeroheating convergence working group in November 2004), but it does provide some confidence that all three tools are working as expected. The peak stagnation point convective heating on this trajectory is predicted to be about 45 W/cm^2, a value in good agreement with design predictions. The estimated uncertainty in this value is approximately 30% based on code validation with Earth entry and ground test data.

Also shown in Fig. 6 is the radiative heat flux computed using NEQAIR and RADEQUIL assuming a Boltzmann distribution, as well as that computed with the CR model. All three computations have been corrected for radiative cooling using Eqs. (1) and (2), and have been corrected for shock curvature effects. Fig. 6 shows that, unlike the agreement seen for convective heating, all three codes give different results for the predicted radiative heating. The highest prediction (RADEQUIL) is over 70 W/cm^2 vs. 45 for NEQAIR and 4.5 for the CR model. Most of the differences between RADEQUIL and NEQAIR are apparently due to differences in the amount of absorption predicted. The RADEQUIL results indicate a nearly optically thin shock layer at all trajectory points, while NEQAIR96 predicts around 20% absorption of the incident radiation at peak heating.

It should be noted again that the results from both RADEQUIL and NEQAIR are considered conservative upper limits on the expected radiative heating. A more accurate assessment of the true radiative heating can be made using the CR model, which is based on experimental data. The peak radiative heating predicted using this method is about 4.5 W/cm^2, which is significantly lower than both the range of design values (35-50 W/cm^2) and the Boltzmann models (45-70 W/cm^2). The estimated uncertainty in this result is approximately 200%, primarily due to the limited amount of available ground test data and the lack of flight heating data for this atmosphere.

6.2 Flank Heating

Fig. 7 shows the computed values of the transition correlation Re_θ/M_e as a function of radial distance from the nose along the Nov. 11 trajectory. Using the specified transition criterion $Re_\theta/M_e = 150$, we see that transition is predicted to occur at about t = 187 s. Transition will commence near the maximum diameter point on the forebody frustum (r > 1.0 m) and travel forward (toward the stagnation point) with time. Fig. 7 shows that the transition front is expected to reach the sphere-cone junction (r = 0.6 m) at about t = 201 s, well after the majority of the heat pulse on this trajectory.

Fig. 8 shows the computed convective and radiative heating at all nine trajectory points at the mid-cone point (r = 0.9 m) on the flank. The flow at the mid-cone point is modeled to be fully turbulent starting at t = 189 s, which causes the jump in the convective heating rate observed in Fig. 8 at this time. Once again all three CFD codes are in good agreement on their predictions of the convective heating levels. Maximum convective heating at the mid-cone point is about 33 W/cm^2 at t = 189 s. The turbulent augmentation factor (increase in heating over the laminar level) at this time is about 1.4.

Once again there are significant differences in the radiative heating predicted by the three tools. However, in all cases we observe that the predicted heating from shock layer radiation at the mid-cone is nearly the same

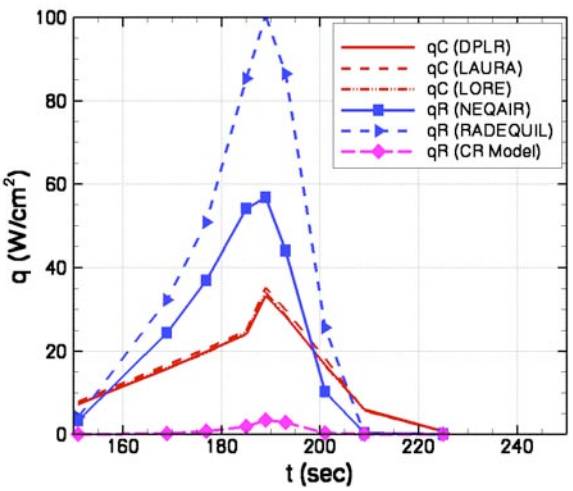

Fig. 8. Computed convective and radiative heating at the mid-cone point along the Nov. 11 trajectory.

as that at the stagnation point. This result is due to offsetting differences; the shock layer at the mid-cone point is cooler, which should lead to less radiation, but both the CN number density and the radiating volume are larger, which lead to increased radiation.

6.3 Integrated Heat Load

Table 2 shows the computed zero-margin convective (Q_C), radiative (Q_R), and total (Q_T) heat loads at the stagnation point and mid-cone point. Results are shown for three simulations: those using DPLR and the CR model (ARC), LAURA and RADEQUIL (LaRC), and LORE (AOES). Note that predictions of shock layer radiation were not performed at AOES, and therefore radiative and total head loads were not computed.

Table 2. Computed Heat Loads in J/cm^2.

	Stag Pt.			Mid-Cone		
	Q_C	Q_R	Q_T	Q_C	Q_R	Q_T
DPLR	2000	70	2070	1275	55	1330
LAURA	2150	2050	4200	1350	2600	3950
LORE	1975	–	–	1275	–	–

All three CFD codes agree within 10% on the predicted total convective heat load. The results from LAURA are slightly (~10%) higher than those of DPLR and LORE due to the use of the supercatalytic (vs. fully catalytic) wall boundary condition.

Total heat loads predicted by DPLR/CR are about 2070 J/cm^2 at the stagnation point and 1330 J/cm^2 at the mid-cone point, as compared to 4200 and 3950 J/cm^2 respectively by LAURA/RADEQUIL. The primary reason for the differences between the two predictions is the radiative heat load, which is predicted to be much smaller using the CR model. As discussed previously the CR model is based on experimental data, and thus is likely a more accurate prediction. The results from RADEQUIL (and NEQAIR, not shown) using an equilibrium model should be considered absolute upper bounds on the radiative heat rates and loads.

Heat loads including uncertainties at the stagnation point are about 2810 J/cm^2 for DPLR/CR and 4845 J/cm^2 for LAURA/RADEQUIL. Note that the LAURA/ RADEQUIL results include zero margin on radiative heating, which is consistent with the assumption that the nominal Boltzmann value represents an upper bound. Once again, the heat load predicted with current tools is within the range of design values.

7. CONCLUSIONS

Although there are unfortunately no flight data with which to compare the predictions, it is still useful to re-assess the heating environment of the Huygens spacecraft using the latest available aerothermal models. The analysis presented herein shows that the predicted convective heating environment is in good agreement with the range of design predictions, while the current best estimate of the radiative heating environment is significantly below design levels. Part of the difference in radiative heating is due to the fact that recent Cassini observations of the Titan atmosphere indicate that there is less atmospheric methane than assumed a decade ago, but a larger portion of the difference is due to the application of a new non-local collisional-radiative model for CN radiation. This model represents the first validated non-equilibrium CN radiation model available in the literature.

8. ACKNOWLEGEMENTS

This work was funded in part by the National Engineering Safety Center Huygens EDL independent assessment activity and the NASA In-Space Propulsion program. The authors thank Jim Robinson, Rafael Molina, Thierry Blanquaert, Steve Labbe, Dick Powell, Mary Kae Lockwood, Dinesh Prabhu, and Christophe Laux for their help and support for this work.

9. REFERENCES

[1] Hollis, B.R, Striepe, S.A, Wright, M.J., Bose, D., Sutton, K., and Takashima, N., "Prediction of the Aerothermodynamic Environment of the Huygens Probe," AIAA Paper No. 2005-4816, Jun. 2005.

[2] Baillion, M., Taquin, G., and Soler, J., "Huygens Radiative Probe Environment," *Proceedings of the 19th International Symposium on Shock Waves*, 1993, pp. 339-346.
[3] Baillion, M. and Taquin, G., "Radiative Heat Flux: Theoretical and Experimental Predictions for Titan Entry Probe," *Capsule Aerothermodynamics*, AGARD Report No. 808, pp. 9/1-9/30, May 1997.
[4] Bose, D., Wright, M.J., Raiche, G.A, Bogdanoff, D., and Allen, G.A., "Modeling and Experimental Validation of CN Radiation Behind a Strong Shock Wave," AIAA Paper No. 2005-0768, Jan. 2005.
[5] Baillion, M., "Aerothermodynamic Requirements and Design of the Huygens Probe," *Capsule Aerothermodynamics*, AGARD Report No. 808, pp. 14/1-14/28, May 1997.
[6] Nelson, H.F., Park, C., and Whiting, E.E., "Titan Atmospheric Composition by Hypervelocity Shock Layer Analysis," *Journal of Thermophysics and Heat Transfer*, Vol. 5, No. 2, 1991, pp. 157-165.
[7] Park, C.S. and Bershader, D., "Studies of Radiative Emission from the Simulated Shock Layer of the Huygens Probe," *Proceedings of the 18th International Symposium on Shock Waves*, 1991, pp. 671-676.
[8] Gökçen, T., "N_2-CH_4-Ar Chemical Kinetic Model for Simulations of Atmospheric Entry to Titan," AIAA Paper No. 2004-2469, Jun. 2004.
[9] Labracherie, L., Billiotte, M., and Houas, L., "Shock Tube Analysis of Argon Influence in Titan Radiative Environment," *Journal of Thermophysics and Heat Transfer*, Vol. 10, No. 1, 1996, pp. 162-168.
[10] Justus, C. and Duvall, A., "Engineering Level Model Atmospheres for Titan and Neptune," AIAA Paper 2003-4803, Jul. 2003.
[11] Lockwood, M.K., "Titan Aerocapture System Analysis," AIAA Paper No. 2003-2799, Jul. 2003.
[12] Wright, M.J., Candler, G.V., and Bose, D., "Data-Parallel Line Relaxation Method for the Navier-Stokes Equations," *AIAA Journal*, Vol. 36, No. 9, 1998, pp. 1603-1609.
[13] Cheatwood, F. and Gnoffo, P., "User's Manual for the Langley Aerothermodynamic Upwind Relaxation Algorithm (LAURA)," NASA TM-4764, Apr. 1996.
[14] Walpot, L., "Development and Application of a Hypersonic Flow Solver," PhD Thesis, T.U. Delft University, May 2002.
[15] Gnoffo, P.A., Gupta, R.N., and Shinn, J.L., "Conservation Equations and Physical Models for Hypersonic Air Flows in Thermal and Chemical Nonequilibrium," NASA TP 2867, Feb. 1989.
[16] Takashima, N., Hollis, B.R., Zoby, E.V., Sutton, K., Olejniczak, J., Wright, M.J., and Prabhu, D.K., "Preliminary Aerothermodynamics Analysis of Titan Aerocapture Aeroshell," AIAA Paper No. 2003-4952, Jul. 2003.
[17] Gupta, R.N., Yos, J.M., Thompson, R.A., and Lee, K., "A Review of Reaction Rates and Thermodynamic and Transport Properties for an 11-Species Air Model for Chemical and Thermal Nonequilibrium Calculations to 30,000 K," NASA RP 1232, Aug. 1990.
[18] Ramshaw, J.D., "Self-Consistent Effective Binary Diffusion in Multicomponent Gas Mixtures," *Journal of Non-Equilibrium Thermodynamics*, Vol. 15, No. 3, 1990, pp. 295-300.
[19] Sutton, K., and Gnoffo, P.A., "Multi-Component Diffusion with Application to Computational Aero-thermodynamics," AIAA Paper No. 98-2575, Jun. 1998.
[20] Baldwin, B. and Lomax, H., "Thin Layer Approximation and Algebraic Model for Separated Turbulent Flows," AIAA Paper No. 78-257, Jan. 1978.
[21] Hollis, B.R., Leichty, D., Wright, M., Holden, M., Wadhams, T., MacLean, M., and Dyakonov, A., "Transition Onset Correlations and Turbulent Heating Measurements for the Mars Science Laboratory Entry Vehicle," AIAA Paper No. 2005-1437, Jan. 2005.
[22] Whiting, E.E., Yen, L., Arnold, J.O., and Paterson, J.A., "NEQAIR96: Nonequilibrium and Equilibrium Radiative Transport and Spectra Program User's Manual," NASA RP-1389, Dec. 1996.
[23] Nicolet, W.E., "User's Manual for the Generalized Radiation Transfer Code (RAD/EQUIL)," NASA CR-116353, Oct. 1969.
[24] Olejniczak, J., Wright, M., Prabhu, D., Takashima, N., Hollis, B., Zoby, E.V., and Sutton, K., "An Analysis of the Radiative Heating Environment for Aerocapture at Titan," AIAA Paper No. 2003-4953, Jul. 2003.
[25] Wright, M.J., Bose, D., and Olejniczak, J., "The Impact of Flowfield-Radiation Coupling on Aeroheating for Titan Aerocapture," *Journal of Thermophysics and Heat Transfer*, Vol. 19, No. 1, 2005, pp. 17-27.
[26] Tauber, M.E. and Wakefield R., "Heating Environment and Protection During Jupiter Entry," *Journal of Spacecraft and Rockets*, Vol. 8, No. 3, 1971, pp. 630-636.
[27] Goulard, R., "The Coupling of Radiation and Convection in Detached Shock Layers," *Journal of Quantitative Spectroscopy and Radiative Heat Transfer*, Vol. 1, 1961, pp. 249-257.
[28] Bose, D. and Wright, M.J., "View-Factor Based Radiation Transport in a Hypersonic Shock Layer," *Journal of Thermophysics and Heat Transfer*, Vol. 18, No. 4, 2004, pp. 553-555.
[29] Gnoffo, P., Weilmuenster, K., Braun, R., and Cruz, C., "Influence of Sonic Line Location on Mars Path-finder Probe Aerothermodynamics," *Journal of Space-craft and Rockets*, Vol. 33, No. 2, 1996, pp. 169-177.